Electronic Supplementary Material (ESI) for Materials Chemistry Frontiers.
This journal is © the Partner Organisations 2023

Supporting Information

Carbon-Regulated Titania Crystallization to Construct a Comprehensive Palette of Anatase/Rutile Mixed Phases for Advanced Photocatalysis

Sijian Ye,[1] Chongling Cheng,[2] Shun Wang,[3] Renguo Xie,[1] and Dayang Wang[1]

1. State Key Laboratory of Inorganic Synthesis and Preparative Chemistry, College of Chemistry, Jilin University, Changchun 130012, P. R. China

2. State Key Laboratory of Bioelectronics, School of Biological Science and Medical Engineering, Southeast University, Nanjing 210096, P. R. China

3. College of Chemistry and Materials Engineering, Institute of New Materials and Industrial Technologies, Key Laboratory of Carbon Materials of Zhejiang Province, Wenzhou University, Wenzhou 325035, China

*Corresponding authors: chengchongling@seu.edu.cn, wangdayang@jlu.edu.cn

Table of Contents

A. Experimental Details ---------- S3

1. Materials
2. Methods
3. Characterization

B. Supplementary Data ---------- S9

1. Preparation of C-Am-TiO_2-X (**Figures S1-S2 and Table S1**)
2. Rietveld refinement results of the crystal unit cells of C-An-TiO_2-X (**Table S2**)
3. ART of as-prepared titania xerogel in air. (**Figure S3**)
4. XPS spectra of as-prepared titania samples. **(Figures S4, S5)**
5. Assessment of the RF values of as-prepared C-An-TiO_2-X in the surface and bulk phase **(Figures S6 - S10)**
6. Comparation of currently available methods for carbon-regulated crystallization of titania **(Table S3)**
7. Study of the CDC effect on ART temperature of as-prepared C-Am-TiO_2-X **(Figure S11)**
8. Rietveld refinement results of the anatase crystal unit cells of as-prepared C-A/R-TiO_2-X **(Table S4)**
9. Crystallographic results of 125 titania samples derived from C-Am-TiO_2-X **(Figures S12 - S16 and Table S5)**
10. Summary of the photocatalytic performance of as-prepared ARM-phase titania for degradation of gaseous acetaldehyde. (**Figures S17 and S18 and Table S6-S10**)

C. References ---------- S39

A. Experimental Details

1. Materials.

Tetratbutyl titanate and acetic acid were purchased from Sigma-Aldrich, Shanghai, China, ethanol was purchased from Sinopharm Chemical Reagent Co., Ltd, and methanol and 5,5-dimethyl-1-pyrroline N-oxide (DMPO) were purchased from Shanghai Aladdin Biochemical Technology Co., Ltd. All reagents were used without further purification. Water with resistivity of 18 $M\Omega \cdot cm^{-1}$ was prepared using a Millipore Milli-Q system and used in all experiments.

2. Methods

2.1 Preparation of TiO_2 xerogels.

Titania xerogels were prepared via acetic acid-catalyzed sol-gel process similar to the protocols reported in literature[S1]. Typically, 6.8g of teratbutyl titanate (0.02 mol) were dissolved in 20 mL of ethanol. Then, the mixture of water (4 mL), ethanol (20 mL), and acetic acid (4.0 g) was dropwise added into the resulting ethanol solution of tertbutyl titanate, which was incubated under ambient conditions under magnetic stirring until the solution were converted into a gel . The resulting gel was dried at 80℃ overnight to yield titania xerogel.

2.2 Preparation of carbon-doped amorphous titania (C-Am-TiO_2).

As-prepared titania xerogels were submitted to a two-step calcination process. Firstly, they underwent calcination in a tube furnace at 300 °C under a continuous argon flow for 2h to convert the xerogels into amorphous titania powders (C-Am-TiO_2) and all organic substances, include acetic acid and butanol, impregnated within the gels into carbon; namely the resulting content was deemed to be the maximum value loaded in the resulting amorphous titania. Subsequently, the resulting carbon-loaded amorphous titania (C-Am-TiO_2) powders were calcined in a Muffle furnace at 300°C in air and the calcination time was altered from 8 h to16, 24 and 32 h to adjust the carbon doping concentration (CDC) in the amorphous titania matrices. The resulting C-Am-TiO_2

powders were specifically denoted as C-Am-TiO_2-X, where X represents the CDC values. The carbon weight fraction in the resulting C-Am-TiO_2 powders were determined by using a carbon-sulfur analyzer (W_c^{mass}, wt%), which were used to calculate the CDC values (X) in terms of molar fraction according to Equation S1:

$$X = \frac{w_c^{mass}/M_c}{w_c^{mass}/M_c + (1 - w_c^{mass})/M_{TiO2}} \times 100 \qquad \text{(S1)}$$

where the molar mass of carbon (M_c) and TiO_2 (M_{TiO_2}) is 12 and 79.9 g·mol^{-1}, respectively.

2.4 Crystallization of as-prepared C-Am-TiO_2-X powders.

As-prepared C-Am-TiO_2-X powders were submitted into calcination in a tube furnace under a continuous argon flow. During calcination, the temperature was firstly elevated to 300℃ at a heating rate of 5 ºC per min and then to targeted calcination temperature of 500℃, 525℃, 550℃, 575℃, 600℃ and 625℃, respectively, at a heating rate of 2 ºC per min, at which the C-Am-TiO_2-X powders were calcined for 10 min, 2h, 4h, 6h and 8h, respectively, to induce the crystallization of the amorphous titania to anatase phase and then anatase/rutile mixed phase. After calcination at a targeted temperature for a given time in argon, the temperature was deliberately reduced to 300℃ at a cooling rate of 2 ºC per min to ensure the homogenous cooling of the resulting samples and gradually reduced to ambient temperature. Note that the entire cooling process was carried out under a continuous argon flow. The resulting carbon-doped anatase phase and anatase/rutile mixed phase titania were denoted as C-An-TiO_2-X and C-A/R-TiO_2-X, respectively.

2.5 Assessment of the crystalline structures of as-prepared C-An-TiO_2 and C-A/R-TiO_2 powders

The XRD patterns of as-prepared C-An-TiO_2-X and C-A/R-TiO_2-X powders were deliberately analyzed with the aid of Software-Jade 6 to assess their crystallinity, the size of their anatase phase, and the size and fraction of the rutile phase structural features. The crystallinity of the resulting titania powders was calculated by using

monocrystalline silicon as the reference for 100% crystallinity. The crystallite size (d) was calculated according to Debye-Scherrer Formula: [S2]

$$d = \kappa\lambda/\beta\cos\theta \quad \text{(S2)}$$

where K is a constant (0.89), λ is the wavelength of X-ray radiation (0.15405 nm), β is the Full width at half maximum (FWHM) of the diffraction peak, and the θ is the Bragg angle. The anatase crystallite sizes of the resulting titania powders was derived from anatase (101) peak at 25.176° (2θ) and their rutile crystallite sizes from rutile (110) peak at 27.355° (2θ). According to the method developed by Spurr and Myers,[S3] the ratio of the weight fraction of the rutile phase (W_R) to that of the anatase phase (W_A) in the resulting C-A/R-TiO_2-X powders was empirically correlated with the intensity ratio of the rutile (110) peak at 27.355° (2θ) (I_R) to the anatase (101) peak at 25.176 (2θ) (I_A), as described in Equation S3

$$\frac{W_R}{W_A} = \frac{W_R}{1-W_R} = 1.22\frac{I_R}{I_A} - 0.028 \quad \text{(S3)}$$

As a result, the weight fraction of the rutile phase of the resulting C-A/R-TiO_2-X powders – simply denoted as rutile fraction (RF) – could be readily calculated according to Equation S3. According to literature,[S4] the Rietveld method was applied to refine the crystal unite cell structures of the resulting C-An-TiO_2-X and C-A/R-TiO_2-X powders with the aid of General Structure Analysis System (GSAS) suite of programs.

2.6 Semiquantitative spatially-differentiated analysis of as-prepared C-A/R-TiO_2 powders by means of Raman Spectroscopy.

The RF values of as-prepared C-A/R-TiO_2-X powders were assessed by means of Raman spectroscopy carried out under UV and visible light irradiation, and the UV Raman signals are known from the surface regions of the ARM phase titania samples and visible Raman signals from their bulk phases. The area ratio of the Raman band of the anatase phase at 400 cm^{-1} to the Raman band of the rutile phase at 445cm^{-1} (I_{400}/I_{445}) was used to quantitatively estimate the weight ratio of the rutile to anatase phase (W_R/W_A). The mixtures of pure anatase and pure rutile powders with defined but varied rutile-to-anatase weight ratios were mechanically ground, which were used to establish the calibration curves of I_{400}/I_{445} as a function of W_R/W_A.

2.7 Study of the photodegradation of gaseous acetaldehyde catalyzed by as-prepared C-An-TiO_2-X and C-A/R-TiO_2-X powders.

As-prepared C-An-TiO_2-X and C-A/R-TiO_2-X powders were used as photocatalysts for degradation of gaseous acetaldehyde under UV light irradiation in a 1 L quartz reactor at 70 °C (343 K) in air with relative humidity of 75%[S5]. A 300 W Xenon lamp (Beijing Perfect light. Co. Ltd.) with a light range of 200–400 nm was used as a UV light source to drive photocatalytic degradation of gaseous acetaldehyde. As-prepared TiO_2 powders (50 mg) were placed on the sample holder in the microreactor at a distance of about 10 cm from the light source. Gaseous acetaldehyde (5 μmol) was quickly injected through the sample inlet into the reactor, corresponding to the concentration of 220 $\mu g \cdot L^{-1}$ in the reactor (1 L). After the equilibrium adsorption of gaseous acetaldehyde into the titania catalysts was reached in a dark environment for 30 min, the reactor was exposed to UV light to induce the photocatalytic acetaldehyde degradation and the total time for each photocatalytic trial was 1h. The concentrations of acetaldehyde and CO_2 in the reactor during photocatalytic acetaldehyde degradation were determined at a time interval of 10 min by means of gas chromatography (GC) equipped with a flame ionization detector (FID). The concentrations of acetaldehyde after equilibrium adsorption was reached in dark (C_{AA}^0), a give time (C_{AA}^t) during photocatalytic degradation and the corresponding CO_2 concentration (C_{CO2}^t) in the reactor were deliberately determined by calibrating the initial acetaldehyde concentration to the original set-up value of 220 $\mu g \cdot L^{-1}$ in the reaction.

The acetaldehyde photocatalytic degradation rate was evaluated by means of pseudo zero-order kinetics model according to Equation S4,

$$C_{AA}^t = C_{AA}^0 - K_0 t \quad \text{(S4)}$$

by means of pseudo first-order kinetics model according to Equation S5:

$$\ln (C_{AA}^0 / C_{AA}^t) = K_1 t \quad \text{(S5)}$$

and by means of pseudo second-order kinetics model according to Equation S6:

$$1/C_{AA}^t - 1/C_{AA}^0 = K_2 t \quad \text{(S6)}$$

The acetaldehyde photocatalytic degradation rate was also evaluated by means of pseudo zero-order kinetics model according to Equation S7:

$$C_{CO_2}^t = K_0 t \quad \text{(S7)}$$

by means of pseudo first-order kinetics model according to Equation S8:

$$\ln (C_{CO_2}^t) = K_1 t \quad \text{(S8)}$$

by means of pseudo second-order kinetics model according to Equation S9:

$$1/C_{CO_2}^t = K_2 t \quad \text{(S9)}$$

Since the fitting coefficients (r^2) of pseudo zero-order kinetics model fitting are closer to 1 than those of other model fittings, here the acetaldehyde photocatalytic degradation and CO_2 formation by as-prepared ARM-phase titania were fitted mainly by using pseudo zero-order kinetics model. Therefore, the degradation rate of acetaldehyde (R_{AA}) was defined by Equation (S10):

$$R_{AA} = k_0 \times \frac{1}{M_{AA}} \times \frac{1}{W_{TiO2}} \quad \text{(S10)}$$

where M_{AA} is the molecular weight of acetaldehyde (44 Da), W_{TiO2} is the amount of titania catalysts (50 mg) and t is the reaction time. Similarly, the formation rate of CO_2 (R_{CO2}) was defined by Equation S11:

$$R_{CO2} = k_0 \times \frac{1}{M_{CO2}} \times \frac{1}{W_{TiO2}} \quad \text{(S11)}$$

where M_{CO2} is the molecular weight of CO_2 (44 Da).

3. Characterization

The CDC values of as-prepared C-Am-TiO_2-X powders were determined by using a carbon-sulfur analyzer (CS230, LECO Corporation, USA) with mg·L-1-level limit of detection. The XRD patterns of as-prepared C-An-TiO_2 and C-A/R-TiO_2 powders were obtained on a X-ray diffractometer (Cu Kα radiation, λ = 1.5406 A) under 40 kV, 200 mA with an angle range of 10-80° and a scanning rate of 0.5°·min^{-1} (2θ) (Empyrean PANalytical B.V. Japan) and the obtained diffraction patterns were analyzed by using Jade XRD libraries and whole pattern fitting. The surface morphology of as-prepared amorphous, anatase, and anatase/rutile mixed phase titania powders and their EDS

pattens were characterized by means of field emission scanning electron microscope (FE-SEM, SU4800, Hitachi, Japan). Transition electron microscopy (TEM) and high-resolution transition electron microscopy (HRTEM) was performed on a JEM 2010F (JEOL, Japan). Thermogravimetric analysis (TGA) and differential scanning calorimetry (DSC) were performed on a thermal analyzer system (NETZSCH STA449F3, Germany) in the temperature range from 50 °C to 500 °C at a heating rate of 5 °C min^{-1} in nitrogen and air, respectively. Thermogravimetric-mass spectroscopy (TGA-MS) was performed on a thermal analyzer system combined with a Mass spectrometer (NETZSCH STA449F3- QMS403D, Germany) in the temperature range from 50 °C to 900 °C at a heating rate of 5 °C min^{-1} in nitrogen and air, respectively. Raman spectroscopy was carried out on a Horiba LabRAM HR evolution instrument in the Raman shift range of 200-800 cm^{-1} under irradiation of 633 nm and 325 nm laser (50 mW), respectively, and the accumulation time of 60 s was applied to collect all the spectroscopic data. Gas chromatography (GC) was performed on an Agilent 7820A GC system (Agilent, U.S.A) equipped with a flame ionization detector. Reactive oxygen species generated on as-prepared C-A/R-TiO_2 under UV irradiation were assessed by means of electron paramagnetic resonance (EPR) spectroscopy by using 5,5-dimethyl-1-pyrroline N-oxide (DMPO) as a spin-trapping agent[S6-S9]. Typically, 5 mg of C-A/R-TiO_2 powder were dispersed in 200 μL of DMPO solutition (100 mM). After 5 min UV irradiation, the resulting suspensions were introduced into capillary quartz tubes to characterize the nature of reactive oxygen species on a JES-FA 200 EPR spectrometer (JEOL, Japan) with an X-band regime (~9.4 GHz) in the magnetic field range of 297~377 mT at room temperature; the EPR spectra of photogenerated •OH radicals were recorded in the aqueous suspensions and those of photogenerated $•O_2^-$ radicals in the methanol suspesions. The EPR spectra of the TiO_2 suspensions obtained without suffering UV irradiation was also measured as control.

B. Supplementary Data

1. Preparation of C-Am-TiO_2-X

Figure S1. (a) Chemical reaction of acetic acid-catalyzed hydrolysis of tetrabutyl titanate . (b) Schematic illustration of calcination of as-prepared titania xerogel powder at 300 °C in argon to form amorphous titania powder with all organic matter completely carbonized (C-Am-TiO_2). The photos of the corresponding powder samples reveal the change in carbon content.

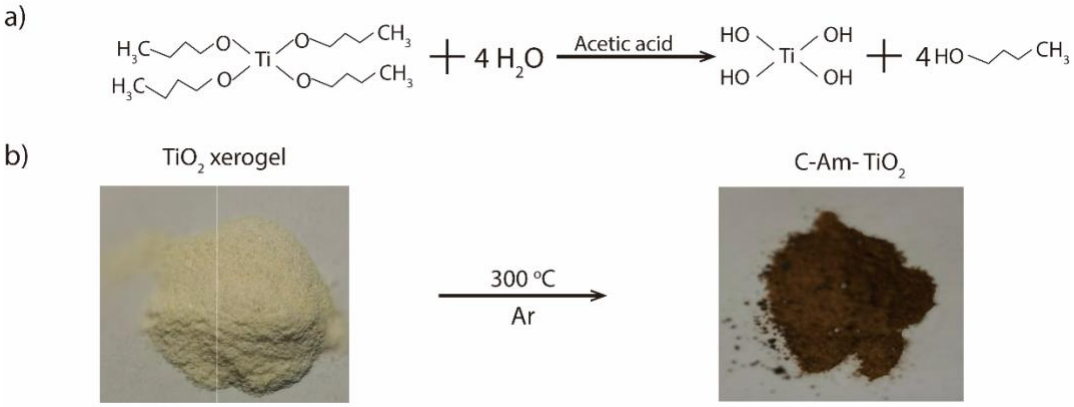

Table S1. Summary of the conditions two-step calcination conditions used to construct C-Am-TiO_2 is calculated according to the equation S1

1st calcination in argon		2nd calcination in air		CDC	
Temperature (°C)	Time (h)	Temperature (°C)	Time (h)	wt.%	mol.%
300	2	0	0	2.72	15.7
300	2	300	8	0.73	4.7
300	2	300	16	0.5	3.2
300	2	300	24	0.44	2.9
300	2	300	32	0.36	2.4

Figure S2. Thermogravimetric analysis (TGA, left curves) and differential scanning calorimetry (DSC, right curves) profiles of C-Am-TiO_2-15.7 (a), C-Am-TiO_2-4.7 (b), C-Am-TiO_2-3.2 (c), C-Am-TiO_2-2.9 (d), C-Am-TiO_2-2.4 (e) in N_2 and C-Am-TiO_2-15.7 in air (f) with the temperature ranging from 50 ºC to 500 ºC at a heating rate of 5 ºC/min.

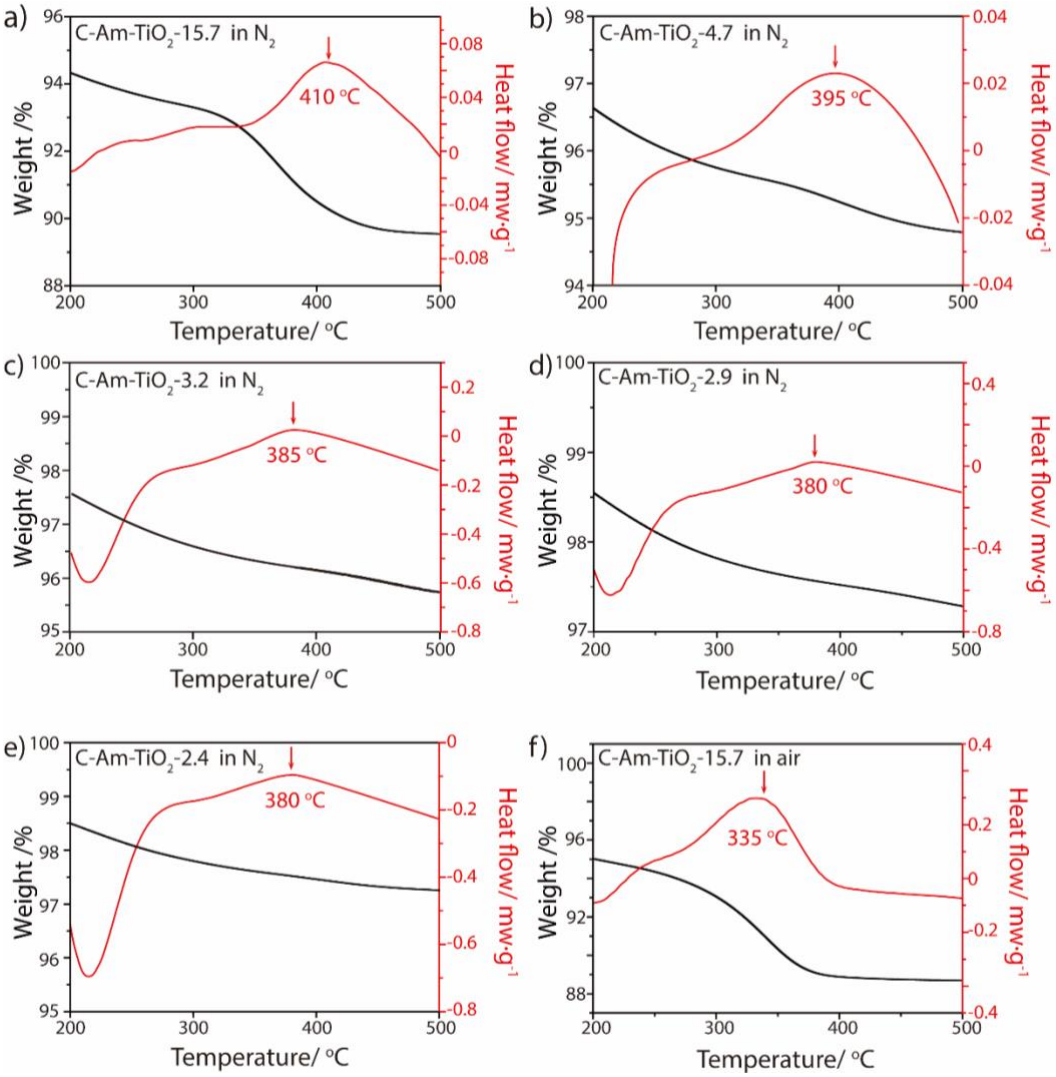

2. Rietveld refinement results of the crystal cell size of as-prepared C-An-TiO_2-X

Table S2. Summary of the anatase crystal unit cell parameters of as-prepared C-An-TiO_2-X powders, obtained after 2h calcination at 500 ºC in argon, which derived from the corresponding XRD patterns refined by the Rietveld method.

CDC (mol %)	Anatase crystal			Fitting Parameters		
	a	b	c	Rp	Rwp	CHi2
15.7	3.787	3.787	9.507	4.97	6.59	0.88
4.7	3. 787	3.787	9.510	5.07	6.78	0.85
3.2	3.787	3.787	9.512	5.86	7.59	1.03
2.9	3.787	3.787	9.512	5.09	6.83	0.89
2.4	3.787	3.787	9.513	4.78	6.49	0.88
0	3.787	3.787	9.52	7.24	9.62	1.53

3. ART of as-prepared titania xerogels in air

Figure S3. XRD patterns of as-prepared titania powders obtained after 2h calcination of titania xerogels in air at 600 ºC (black curve) and 625 ºC (red curve), respectively.

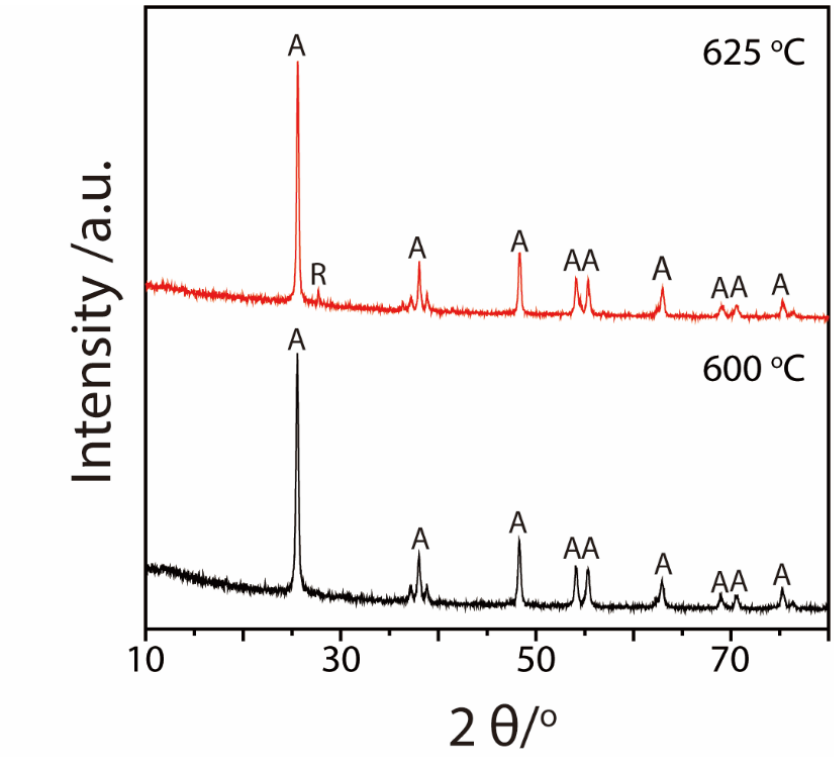

4. XPS spectra of as-prepared titania samples.

Figure S4. XPS spectra of the Ti signals of as-prepared titania samples obtained by 2h calcination of titania xerogel at 550 °C in air (a) and 2 h calcination of C-Am-TiO_2 -2.4 (b), C-Am-TiO_2 -4.7 (c), and C-Am-TiO_2 -15.7 (d) at 550 °C in argon. The sample obtained by 2h calcination of titania xerogel at 550 °C in air represents the carbon-doped titania with CDC of 0 mol %. The absence of Ti^{3+} signals in all these titania samples indicates there is no oxygen vacancy formed during calcination.

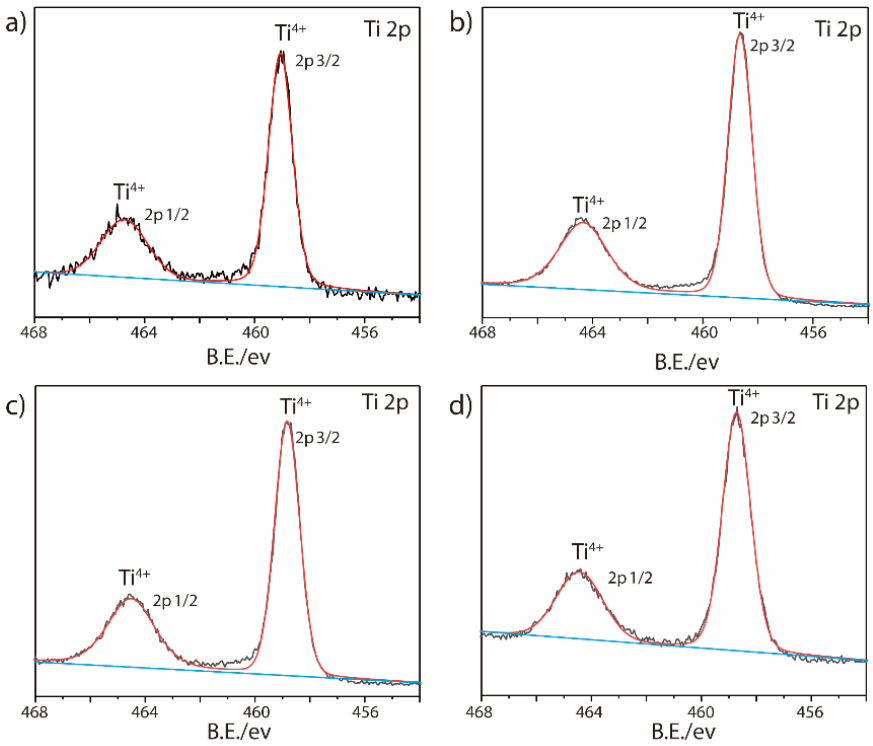

Figure S5. High-resolution XPS spectra of the C signals of as-prepared titania samples obtained by 2h calcination of titania xerogel at 550 °C in air (a) and 2 h calcination of C-Am-TiO_2 -2.4 (b), C-Am-TiO_2 -4.7 (c), and C-Am-TiO_2 -15.7 (d) at 550 °C in argon. The sample obtained by 2h calcination of titania xerogel at 550 °C in air represents the carbon-doped titania with CDC of 0 mol %. The absence of C-Ti signals in all these titania samples indicates there is no carbon infused into the titania network during calcination.

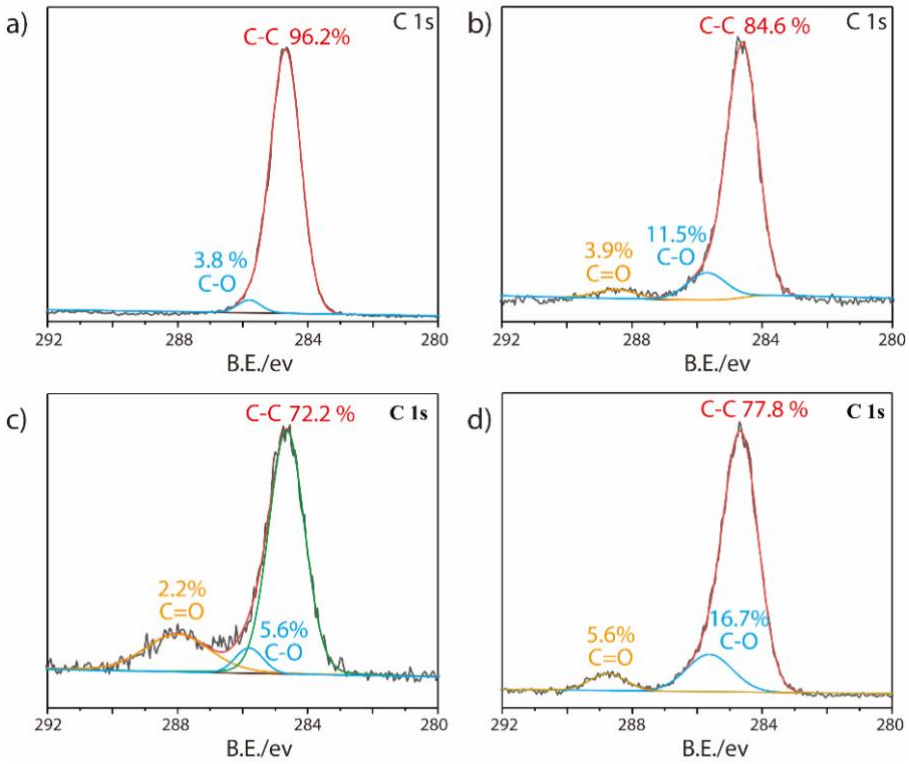

5. Assessment of the RF values of as-prepared C-A/R-TiO_2-X in the surface and bulk phase

Figure S6. (a, b) Raman spectra of the mixtures of pure anatase and pure rutile with the rutile fraction (RF) of 9.1, 28.6, 50, 71.4, and 90.1, obtained under irradiation of visible (a) and UV light (b). The characteristic Raman bands assigned to anatase and rutile are highlighted by blue and red dashed lines, respectively, and marked by A and R. (c, d) Plot of the ratio of the area of the Raman band of anatase at 400 cm^{-1} (I_{400}) to the sum of I_{400} and the area of the Raman band of rutile at 445 cm^{-1} (I_{445}), namely, $I_{400} + I_{445}$, obtained under visible (c) and UV (d) light irradiation, versus of the RF values, which can be well fitted with linear functions (marked).

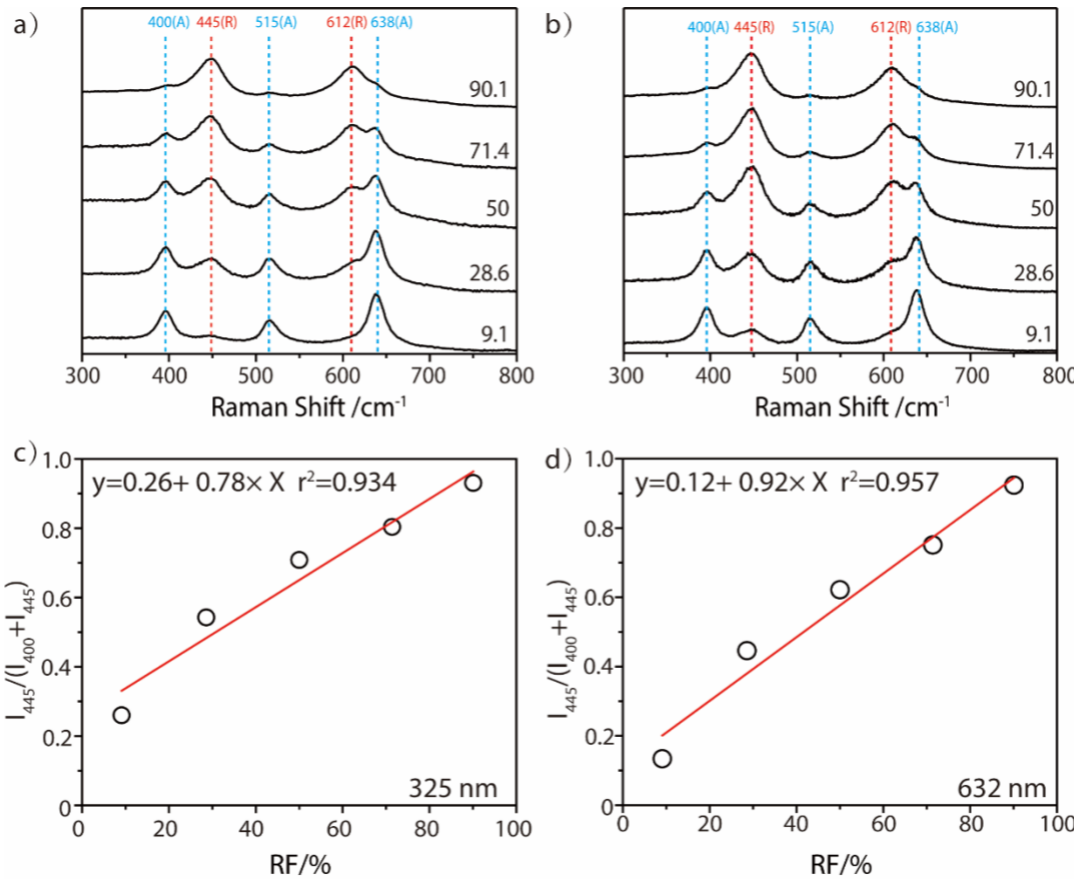

Figure S7. Raman spectra of as-preapred C-A/R-TiO_2 -X with CDC of 15.7 mol% (a, b); 4.7 mol% (c, d); 3.2 mol% (e, f), 2.9 mol% (g, h), and 2.4 mol% (i, j) in argon. The Raman spectra are obtained under irradiation of visible (a, c, e, g, i) and UV light (b, d, f, h, j), in which the characteristic Raman bands of anatase (A) and rutile (R) are marked.

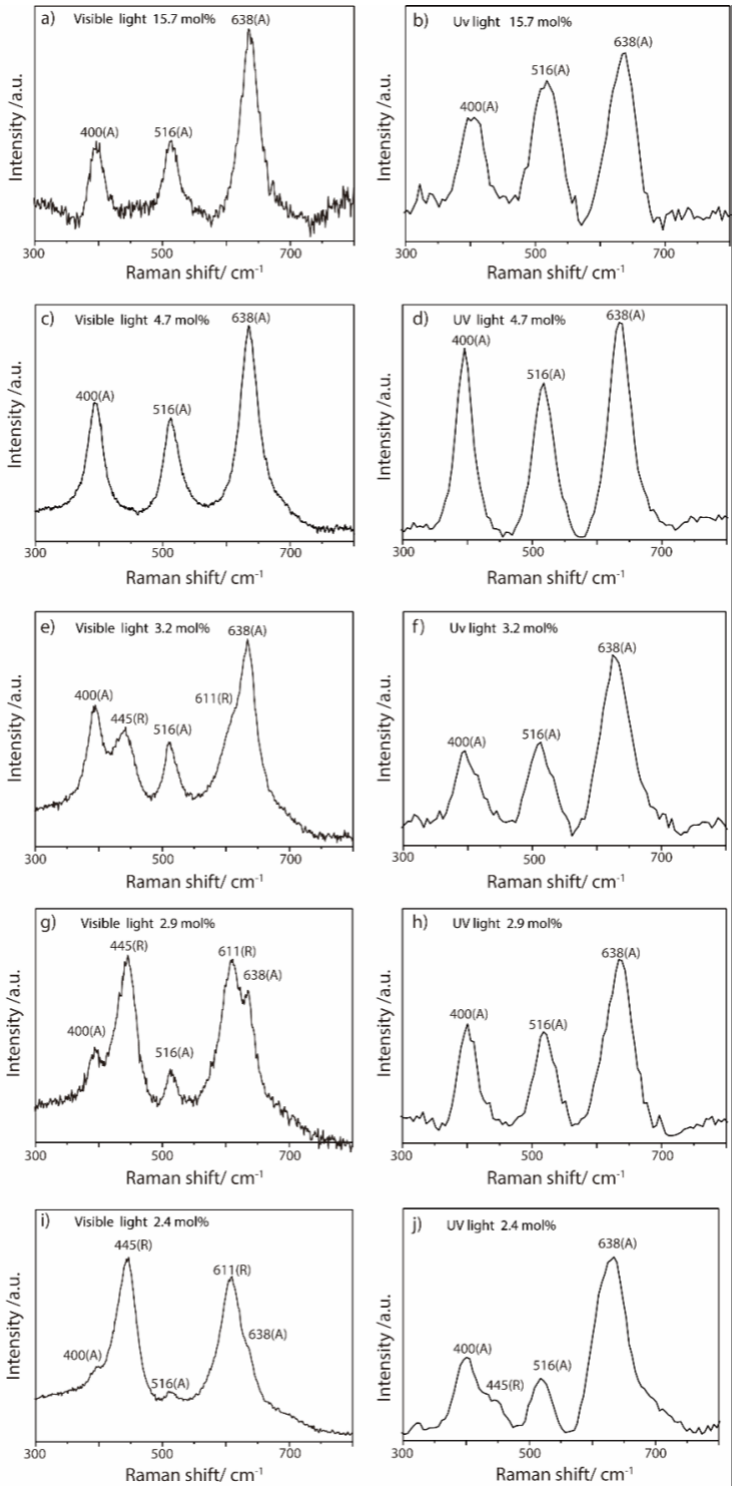

Figure S8. Raman spectra of as-prepared C-A/R-TiO_2-3.2 obtained by 2 h calcination of the corresponding C-Am-TiO_2-3.2 at 525 ^oC (a, b) 550 ^oC (c, d) , 575 ^oC (e, f) , 600 ^oC (g, h) and 625 ^oC (i, j) in argon. The Raman spectra are obtained under irradiation of visible (a, c, e, g, i) and UV light (b, d, f, h, j), in which the characteristic Raman bands of anatase (A) and rutile (R) are marked.

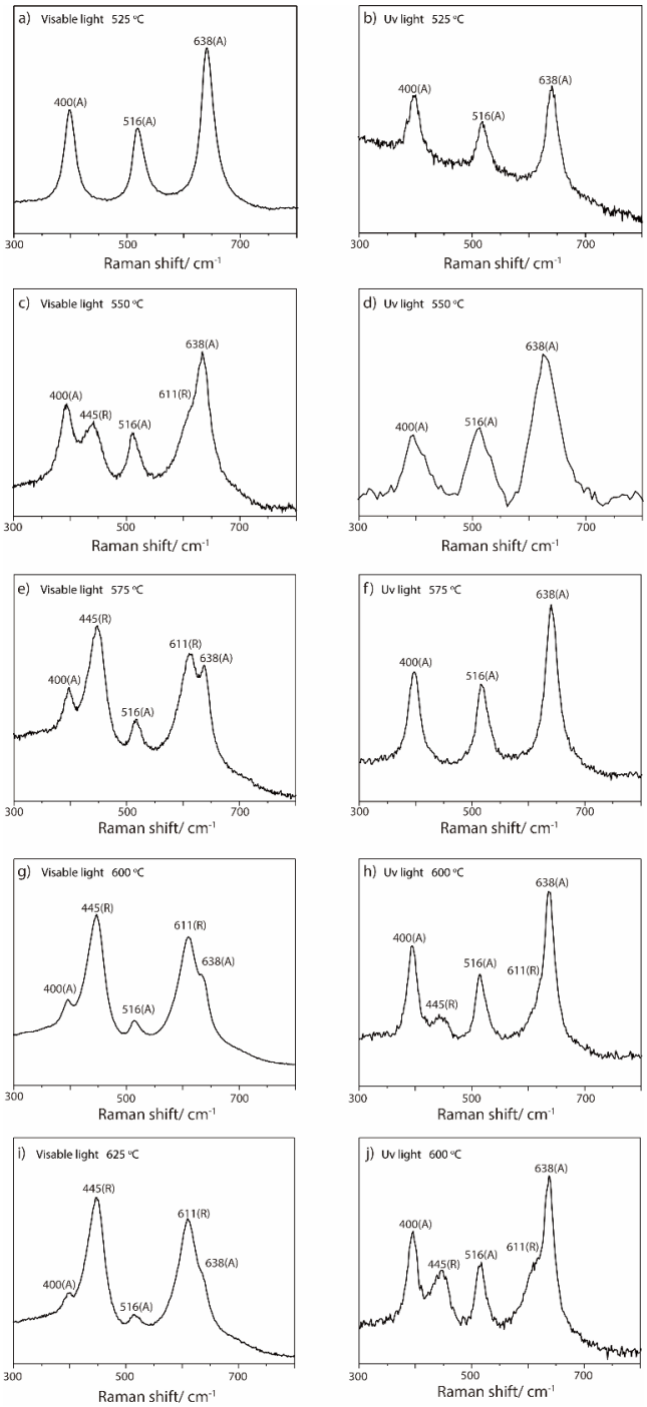

Figure S9. (a) XRD patterns of as-prepared C-A/R-TiO_2-X samples obtained after 2h calcination of the corresponding C-Am-TiO_2-X precursors at 550 ºC in argon. (b) the XRD patterns of as-prepared C-A/R-TiO_2-3.2 obtained by 2 h calcination of the corresponding C-Am-TiO_2-3.2 at temperature ranging from 525 ºC to 625 ºC in argon.

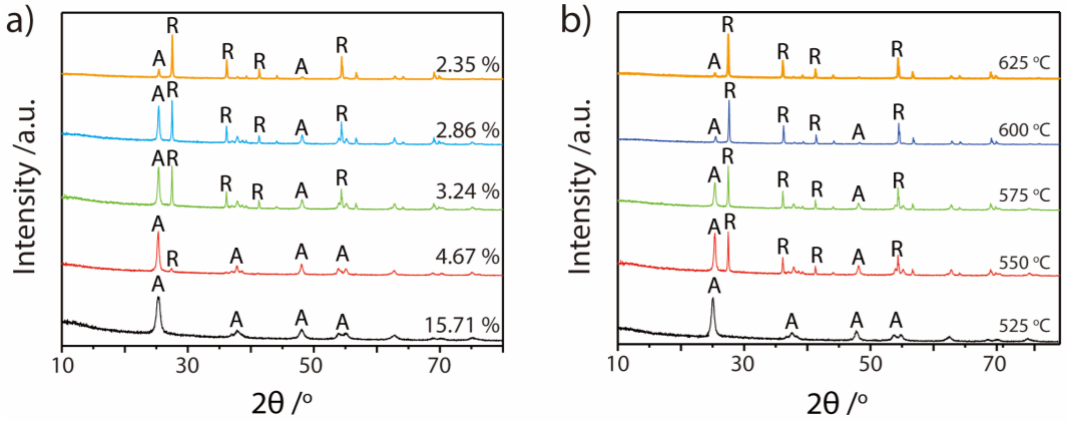

Figure S10. (a) Visible and (b) UV Raman spectra of as-prepared C-An-TiO_2-15.7 obtained by 2 h calcination of the corresponding C-Am-TiO_2-15.7 at 550 ºC in argon. The vibrational bands of carbon at 1350 and 1600 cm^{-1} are observed in the visible Raman spectrum but not in the UV light Raman spectrum.

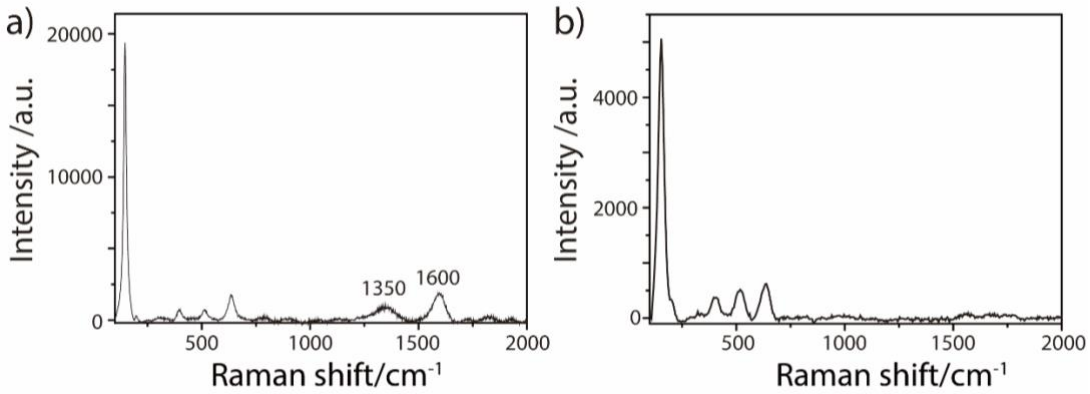

6. Comparation of currently available methods for carbon-regulated crystallization of titania

Table S3. Summary of the calcination environmental nature and ART temperature reported for carbon-regulated crystallization of titania in literature and the anatase size of the resulting titania. Note that here the ART temperature is hypothesized to be above the highest temperature used for growth of anatase reported in the cited references, provided there is no clear evidence of ART in the references.

	Calcination atmosphere	ART temperature (°C)	Anatase size (nm)	References
1	Argon	525℃	14.5 nm	*This work*
2	Argon	900℃	---	*S9*
3	Argon	600℃	---	*S10*
4	Air	600℃	---	*S11*
5	Argon	Above 800℃	---	*S12*
6	Argon	Above 800℃	---	*S13*
7	Argon	700℃	---	*S14*
8	Nitrogen	700℃	---	*S15*
9	Vacuum under 6.5Pa	700℃	31.5 nm	*S16*
10	Air	800℃	---	*S17*
11	Argon	Above 700℃	---	*S18*
12	Argon	Above 750℃	---	*S19*
13	Argon	Above 750℃	---	*S20*

14	Argon	Above 800℃	---	*S21*
15	Argon	800℃	20 nm	*S22*

7. Study of the CDC effect on ART temperature of as-prepared C-Am-TiO_2-X

Figure S11. XRD patterns of as-prepared C-Am-TiO_2-15.7 a), C-Am-TiO_2-4.7 b), and C-Am-TiO_2-2.4 c) obtained after 2 h calcination in argon at temperature ranging from 500 ºC to 625 ºC.

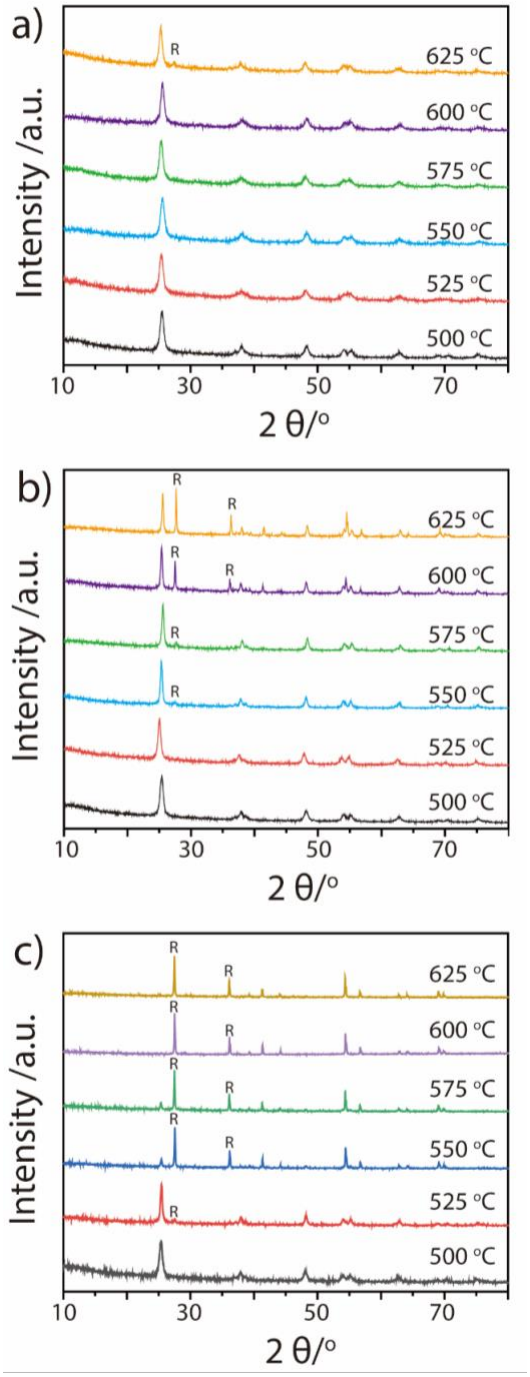

8. Rietveld refinement results of the anatase crystal unit cells of as-prepared C-A/R-TiO_2-X

Table S4. Summary of the anatase unit cell sizes of the C-A/R-TiO_2-X samples obtained after 2h calcination of the corresponding C-Am-TiO_2-X precursors at 600 °C in argon. The crystal unite cell structures are refined by using the Rietveld method.

CDC (mol%)	RF (%)	Anatase phase			Rutile phase			Fitting Parameters		
		a	b	c	a	b	c	Rp	Rwp	CHi2
15.7	0	3.781	3.781	9.498				4.97	6.59	0.88
4.7	46	3.784	3.784	9.516	4.594	4.594	2.959	5.07	6.78	0.85
3.2	89.6	3.784	3.784	9.516	4.594	4.594	2.959	5.86	7.59	1.03
2.9	79.3	3.785	3.785	9.519	4.594	4.594	2.959	5.09	6.83	0.89
2.4	97.7	3.789	3.788	9.520	4.594	4.594	2.959	4.78	6.49	0.88
0	0	3.788	3.787	9.525				7.24	9.62	1.53

9. Crystallographic results of 125 titania samples derived from C-Am-TiO_2-X

Figure S12. XRD patterns of 25 titania samples derived from calcination of C-Am-TiO_2-15.7 at 525 °C (a), 550 °C (b), 575 °C (c), 600 °C (d), and 625 °C (e), respectively, in argon for 10 min (black curves), 2 h (red curves), 4 h (blue curves), 6 h (green curves), 8 h (pink curves). Note that the calcination time of 10 min represents the scenario where calcination stops immediately after the targeted calcination temperature is reached.

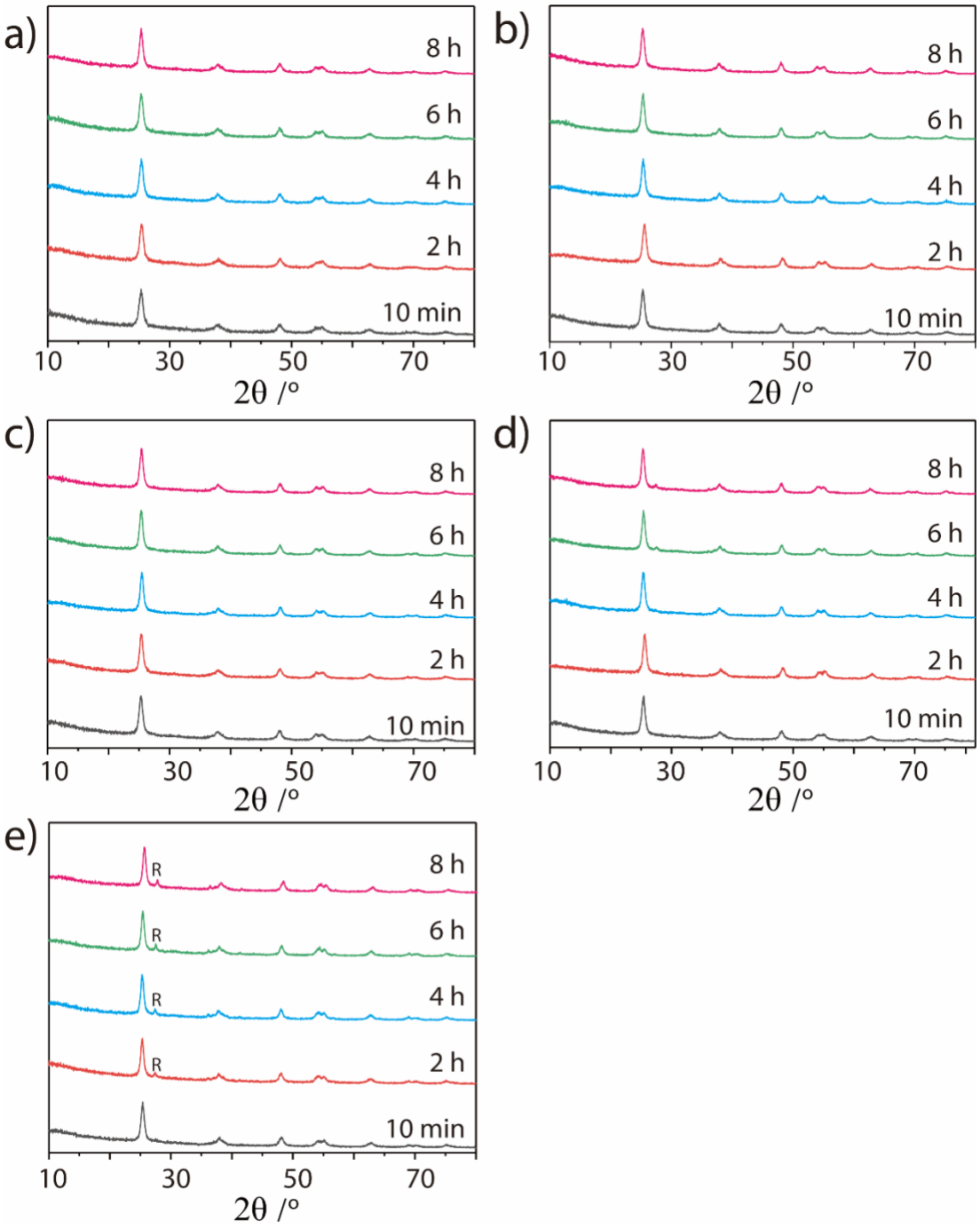

Figure S13. XRD patterns of 25 titania samples derived from calcination of C-Am-TiO_2-4.7 at 525 °C (a), 550 °C (b), 575 °C (c), 600 °C (d), and 625 °C (e), respectively, in argon for 10 min (black curves), 2 h (red curves), 4 h (blue curves), 6 h (green curves), 8 h (pink curves). Note that the calcination time of 10 min represents the scenario where calcination stops immediately after the targeted calcination temperature is reached.

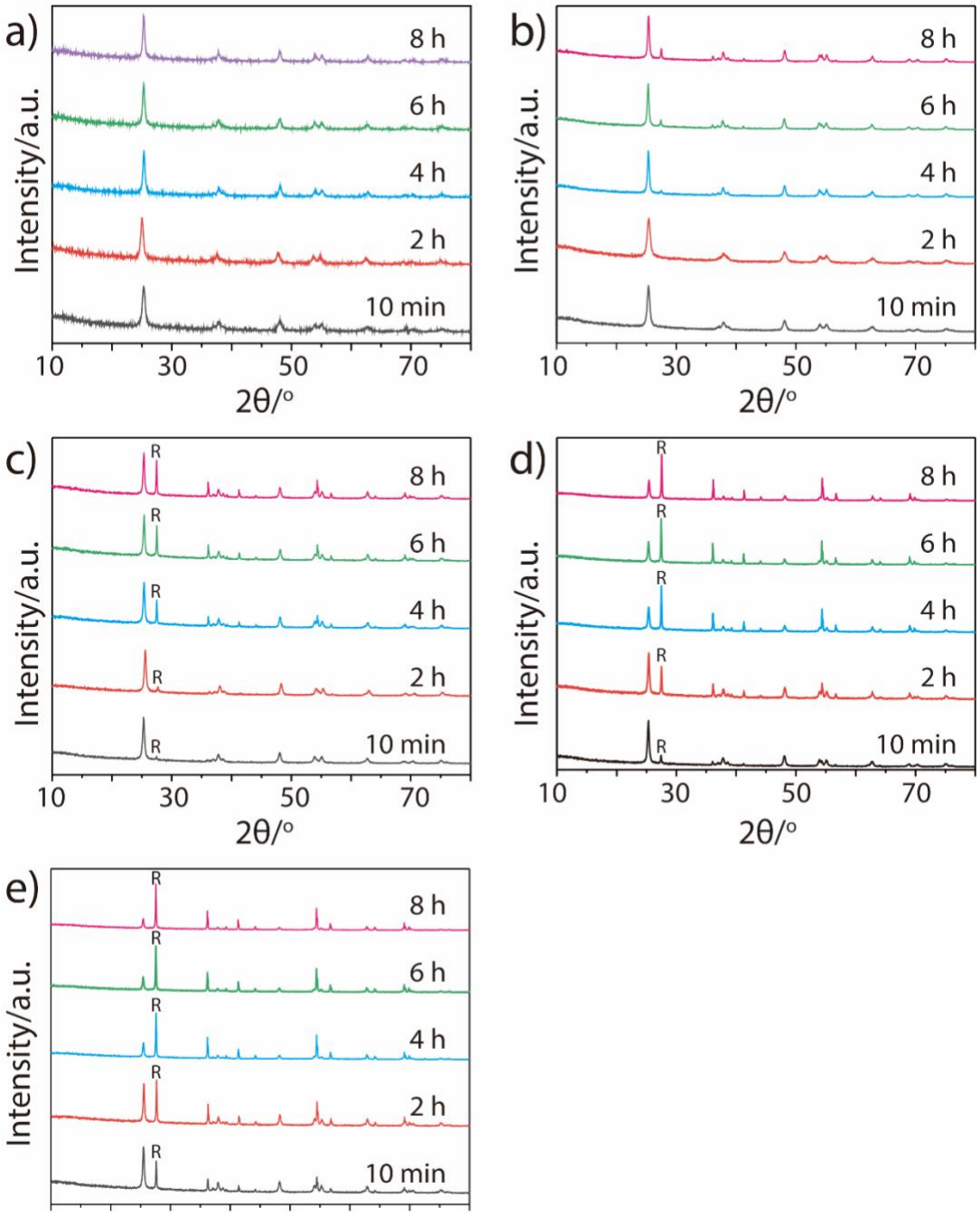

Figure S14. XRD patterns of 25 titania samples derived from calcination of C-Am-TiO_2-3.2 at 525 °C (a), 550 °C (b), 575 °C (c), 600 °C (d), and 625 °C (e), respectively, in argon for 10 min (black curves), 2 h (red curves), 4 h (blue curves), 6 h (green curves), 8 h (pink curves). Note that the calcination time of 10 min represents the scenario where calcination stops immediately after the targeted calcination temperature is reached.

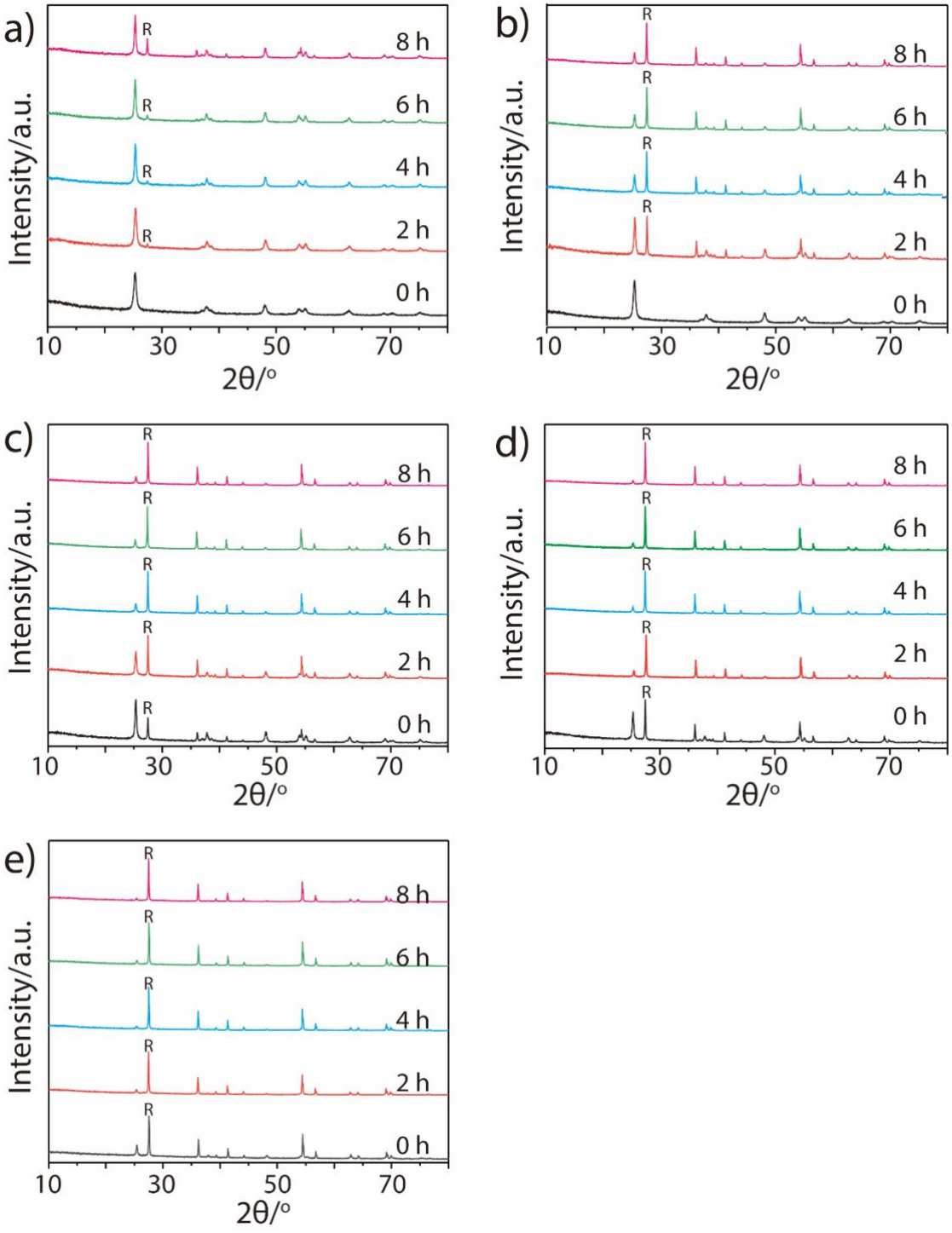

Figure S15. XRD patterns of 25 titania samples derived from calcination of C-Am-TiO_2-2.9 at 525 °C (a), 550 °C (b), 575 °C (c), 600 °C (d), and 625 °C (e), respectively, in argon for 10 min (black curves), 2 h (red curves), 4 h (blue curves), 6 h (green curves), 8 h (pink curves). Note that the calcination time of 10 min represents the scenario where calcination stops immediately after the targeted calcination temperature is reached.

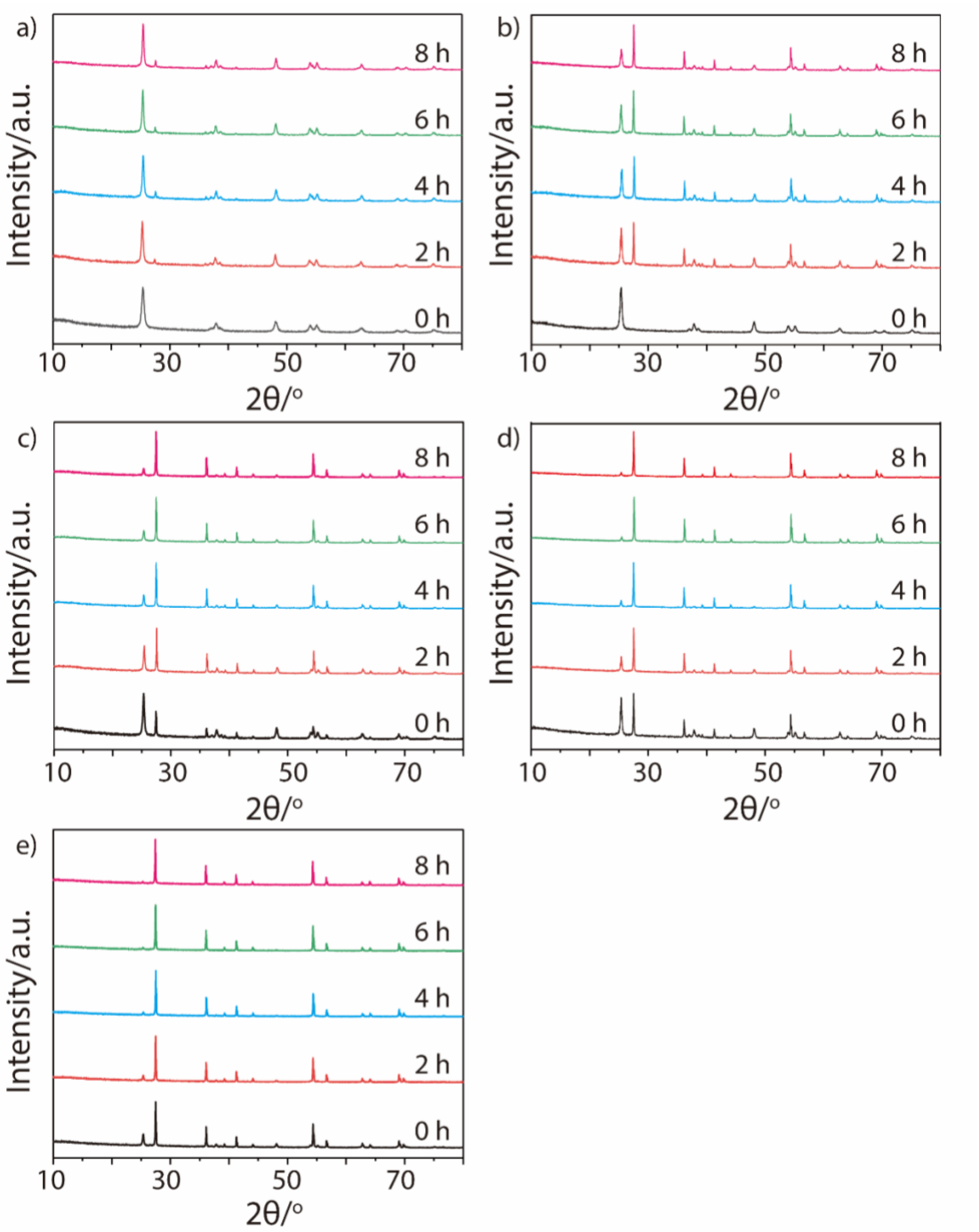

Figure S16. XRD patterns of 25 titania samples derived from calcination of C-Am-TiO_2-2.4 at 525 °C (a), 550 °C (b), 575 °C (c), 600 °C (d), and 625 °C (e), respectively, in argon for 10 min (black curves), 2 h (red curves), 4 h (blue curves), 6 h (green curves), 8 h (pink curves). Note that the calcination time of 10 min represents the scenario where calcination stops immediately after the targeted calcination temperature is reached.

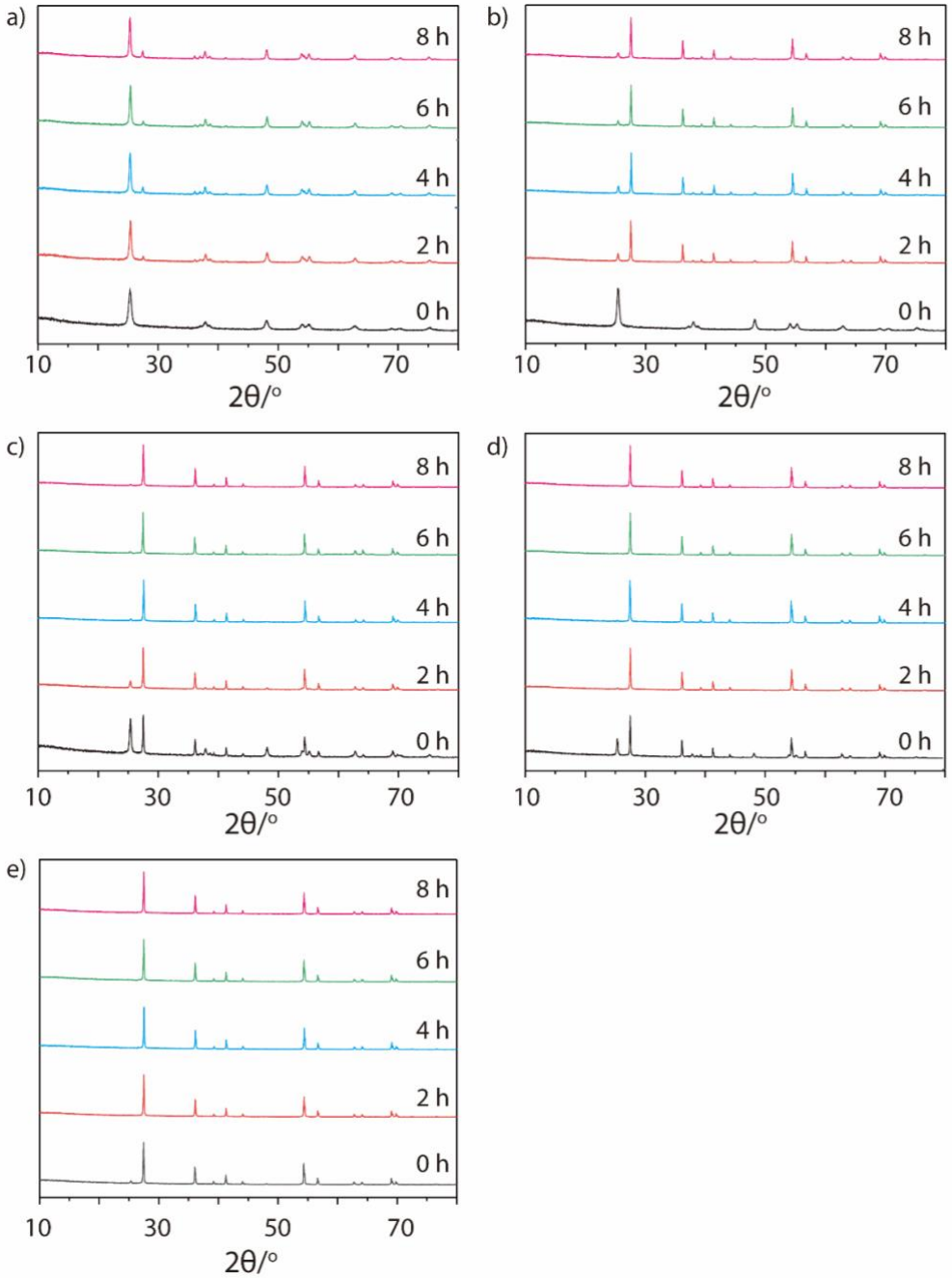

Table S5. Summary of the anatase sizes, the rutile sizes and the RF values of 125 titania samples obtained via calcination of C-Am-TiO_2-X in argon. The temperature and time of calcination are systematically altered and listed in the table.

CDC (mol %)	Calcination Temperature (°C)	Time (h)	RF (%)	Anatase phase size (nm)	Rutile phase size (nm)
15.7	500	0	0	11.0	0
15.7	500	2	0	11.6	0
15.7	500	4	0	13.2	0
15.7	500	6	0	13.4	0
15.7	500	8	0	13.7	0
15.7	525	0	0	11.3	0
15.7	525	2	0	12.2	0
15.7	525	4	0	12.8	0
15.7	525	6	0	13.0	0
15.7	525	8	0	14.3	0
15.7	550	2	0	12.9	0
15.7	550	4	0	13.7	0
15.7	550	6	0	13.9	0
15.7	550	8	0	14.1	0
15.7	575	0	0	12.8	0
15.7	575	2	0	13.3	0
15.7	575	4	0	13.6	0
15.7	575	6	0	13.7	0
15.7	575	8	0	14.1	0
15.7	600	0	0	13.9	0
15.71	600	2	0	14.2	0
15.7	600	4	0	14.4	0
15.7	600	6	10.4	14.5	18.4
15.7	600	8	11.6	15.4	18.2
15.7	625	0	6.4	14.7	32.9

15.7	625	2	12.5	14.9	20.3
15.7	625	4	13.9	15.3	20.2
15.7	625	6	16.5	15.2	23.6
15.7	625	8	17.9	15.7	26.1
4.7	500	0	0	13.2	0
4.7	500	2	0	14.3	0
4.7	500	4	0	15.3	0
4.7	500	6	0	15.3	0
4.7	500	8	0	16.4	0
4.7	525	0	0	15.3	0
4.7	525	2	0	16.6	0
4.7	525	4	0	19.5	0
4.7	525	6	5.2	20.0	17.5
4.7	525	8	5.3	20.3	26.0
4.7	575	0	9.1	21.4	26.3
4.7	575	2	13.5	21.8	30.2
4.7	575	4	41.8	23.1	47.3
4.7	575	6	48.6	25.2	48.1
4.7	575	8	51.9	25.1	49.6
4.7	600	0	19.2	23.5	37.4
4.7	600	2	46	24.0	45.2
4.7	600	4	71.5	25.2	53.2
4.7	600	6	73	26.8	54.3
4.7	600	8	75.8	29.7	53.2
4.7	625	0	45.8	24.4	46.8
4.7	625	2	58.3	28.7	49.9
4.7	625	4	79.5	29.1	52.5
4.7	625	6	81.6	29.5	52.9
4.7	625	8	85.8	29.8	55.8
3.2	500	0	0	13.4	0
3.2	500	2	0	16.4	0
3.2	500	4	0	16.6	0
3.2	500	6	0	17.0	0

3.2	500	8	0	17.6	0
3.2	525	0	0	15.6	0
3.2	525	2	0	17.5	0
3.2	525	4	9.3	22.3	19.5
3.2	525	6	12.9	22.3	29.7
3.2	525	8	34.6	23.8	41.7
3.2	575	0	40.1	23.0	40.6
3.2	575	2	68	24.9	47.9
3.2	575	4	85.8	26.2	53.2
3.2	575	6	86.4	27.2	52.5
3.2	575	8	88.6	30.4	53.2
3.2	600	0	65.2	26.5	48.7
3.2	600	2	89.6	29.4	49.0
3.2	600	4	90	33.8	52.5
3.2	600	6	91.5	27.0	56.6
3.2	600	8	93.7	24.6	54.6
3.2	625	0	82.9	26.5	48.7
3.2	625	2	93.6	30.8	53.9
3.2	625	4	93.5	26.2	51.9
3.2	625	6	95.5	24.3	52.5
3.2	625	8	96	24.0	55.8
2.9	500	0	0	14.2	0
2.9	500	2	0	16.7	0
2.9	500	4	0	16.8	0
2.9	500	6	0	16.9	0
2.9	500	8	0	17.5	0
2.9	525	0	0	16.67	0
2.9	525	2	12.1	22.2	35.9
2.9	525	4	13.7	22.9	38.0
2.9	525	6	16.3	24.9	40.4
2.9	525	8	17.1	25.0	42.3
2.9	550	8	75	28.2	55.0
2.9	575	0	41.9	24.5	49.0

2.9	575	2	68	29.8	52.5
2.9	575	4	83	30.3	55.0
2.9	575	6	84.6	29.5	55.4
2.9	575	8	89.3	30.6	59.9
2.9	600	0	58.7	26.9	51.2
2.9	600	2	79.3	33.8	57.3
2.9	600	4	90.4	33.7	56.5
2.9	600	6	93.2	34.4	56.1
2.9	600	8	94.4	31.0	57.7
2.9	625	0	83.1	28.8	57.0
2.9	625	2	91.9	32.3	58.6
2.9	625	4	95.2	29.8	59.0
2.9	625	6	96.7	28.3	57.4
2.9	625	8	97.2	29.2	60.3
2.4	500	0	0	15.2	0
2.4	500	2	0	17.3	0
2.4	500	4	0	17.4	0
2.4	500	6	0	17.7	0
2.4	500	8	0	18.3	0
2.4	525	0	0	16.5	0
2.4	525	2	11.4	22.4	32.7
2.4	525	4	11.7	25.6	37.6
2.4	525	6	15.5	25.8	35.6
2.4	525	8	17.5	28.2	36.3
2.4	575	0	58.2	24.7	45.1
2.4	575	2	88.3	29.8	52.5
2.4	575	4	96.2	25.1	53.2
2.4	575	6	96.9	24.0	52.1
2.4	575	8	98	19.9	52.5
2.4	600	0	74.7	30.8	55.0
2.4	600	2	97.7	29.6	54.6
2.4	600	4	98.3	25.2	52.1
2.4	600	6	100	0	52.1

2.4	600	8	100	0	54.2
2.4	625	0	95.8	27.2	52.9
2.4	625	2	100	0	56.6
2.4	625	4	100	0	55.0
2.4	625	6	100	0	53.9
2.4	625	8	100	0	55.4

10. Photocatalytic performance of as-prepared ARM-phase titania

Table S6. Summary of the experimental results of degradation rate (k_{AA}) of gaseous acetaldehyde by as-prepared ARM-phase titania with various RF but similar anatase size. The fitting results are obtained according to pseudo-zero-order (Equation S4), pseudo-first-order (Equation S5) and pseudo-second-order kinetics models (Equation S6), respectively.

RF %	pseudo zero-order kinetics model		pseudo first-order kinetics model		pseudo second-order kinetics model	
	K_0	r^2	K_1	r^2	K_2	r^2
0.0	0.88	0.998	0.0048	0.995	$2.63*10^{-5}$	0.989
16.3	1.29	0.994	0.0075	0.992	$4.48*10^{-5}$	0.982
40.1	1.10	0.994	0.0064	0.998	$3.76*10^{-5}$	0.996
58.2	1.05	0.995	0.0061	0.998	$3.52*10^{-5}$	0.997
98.0	0.50	0.991	0.0025	0.953	$1.21*10^{-5}$	0.984

Table S7. Summary of the experimental results of CO_2 formation (k_{CO_2}) of gaseous acetaldehyde by as-prepared ARM-phase titania with various RF (%) but similar anatase size. The fitting results are obtained according to pseudo-zero-order (Equation S7), pseudo-first-order (Equation S8) and pseudo-second-order kinetics models (Equation S9), respectively.

RF %	pseudo zero-order kinetics model		pseudo first-order kinetics model		pseudo second-order kinetics model	
	K_0	r^2	K_1	r^2	K_2	r^2
0	0.995	0.999	0.035	0.946	0.0015	0.784
16.3	1.704	0.998	0.037	0.947	0.0010	0.782
40.1	1.498	0.999	0.035	0.946	0.0010	0.788
58.2	1.557	0.999	0.035	0.940	0.0010	0.770
98.0	0.880	0.999	0.033	0.945	0.0016	0.793

Table S8. Summary of the experimental results of degradation rate (k_{AA}) of gaseous acetaldehyde by as-prepared ARM-phase titania with various RF but similar anatase size. The fitting results are obtained according to pseudo-zero-order (Equation S4), pseudo-first-order (Equation S5) and pseudo-second-order kinetics models (Equation

S6), respectively.

Anatase size (nm)	pseudo zero-order kinetics model		pseudo first-order kinetics model		pseudo second-order kinetics model	
	K_0	r^2	K_1	r^2	K_2	r^2
14.9	0.704	0.996	0.0037	0.998	$1.98*10^{-5}$	0.998
21.8	0.658	0.984	0.0035	0.977	$1.86*10^{-5}$	0.968
24.9	1.281	0.994	0.0075	0.992	$4.48*10^{-5}$	0.982
28.2	0.992	0.998	0.0055	0.993	$3.06*10^{-5}$	0.993

Table S9. Summary of the experimental results of CO_2 formation (k_{CO_2}) of gaseous acetaldehyde by as-prepared ARM-phase titania with various RF but similar anatase size. The fitting results are obtained according to pseudo-zero-order (Equation S7), pseudo-first-order (Equation S8) and pseudo-second-order kinetics models (Equation S9), respectively.

Anatase size (nm)	pseudo zero-order kinetics model		pseudo first-order kinetics model		pseudo second-order kinetics model	
	K_0	r^2	K_1	r^2	K_2	r^2
14.9	0.740	0.999	0.032	0.962	0.0017	0.832
21.8	0.892	0.999	0.033	0.952	0.0015	0.800
24.9	1.704	0.998	0.037	0.947	0.0010	0.782
28.2	1.400	0.992	0.025	0.979	0.0006	0.903

Figure S17. (a, b) Temporal evaluation of photocatalytic acetaldehyde degradation (C_{AA}^{t} , a) and CO_2 formation (C_{CO2}^{t} , b) of as-prepare ARM-phase titania samples with comparable anatase sizes in the range of 20 - 24 nm and rutile sizes in the range of 40 – 53 nm but the RFs being varied from 0% (squares) to 16.% (circles), 40% (upper triangles), 58%(down triangles), 98% (diamonds), which are fitted according to pseudo-zero-order model. **(c, d)** Temporal evaluation of photocatalytic acetaldehyde degradation (C_{AA}^{t} , c) and CO_2 formation ($C_{CO_2}^{t}$, d) of of as-prepare ARM-phase titania with comparable rutile sizes in the range of 21 – 40 nm and RFs in the range of 12.5-17.5% but anatase sizes being varied from 14.9 nm (squares), 21.8 nm (upper triangles), 24.9 nm (circles), 28.2 nm (down triangles), which are fitted according to pseudo-zero-order model.

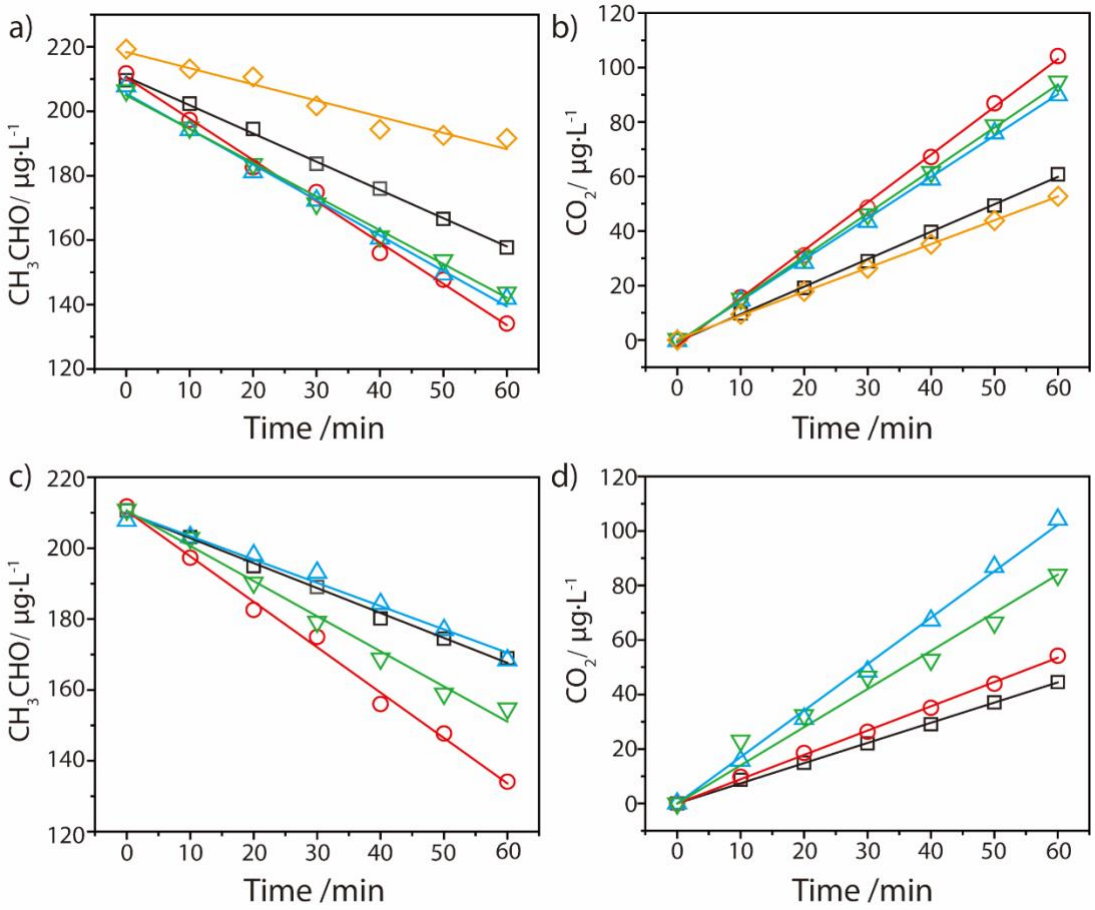

Table S10. Summary of the structural features of as-prepared ARM-phase titania used for photocatalysis of degradation of gaseous acetaldehyde, the corresponding rates of acetaldehyde degradation (R_{AA}) of and CO_2 formation (R_{CO2}) the CDC values of their C-Am-TiO_2-X precursor, and the calcination temperatures and times used to produce the ARM-phase titania.

CDC (mol%)	Calcination temperature (°C)	Calcination time (h)	RF (%)	Anatase size (nm)	Rutile size (nm)	R_{AA} ($\mu mol \cdot g^{-1} \cdot h^{-1}$)	R_{CO2} ($\mu mol \cdot g^{-1} \cdot h^{-1}$)
4.7	525	4	0.0	19.5	0.0	23.9	27.1
2.9	525	6	16.3	24.9	40.4	34.9	46.5
4.7	575	0	40.1	23.00	40.6	27.5	40.9
2.4	575	0	58.2	24.7	45.1	28.6	42.5
2.4	575	8	98.0	19.9	52.5	13.7	24.0
15.7	625	2	12.5	14.9	20.5	19.2	20.2
4.7	575	2	13.5	21.8	30.2	18.0	24.3
2.9	525	6	16.3	24.9	40.4	34.9	46.5
2.4	525	8	17.5	28.1	36.3	27.1	38.2

Figure S18. EPR spectra of the reactive oxygen species generated after C-A/R-TiO_2-2.9 powder are treated with (red curves) and without 5 min UV irradiation (black curves); the photogenerated •OH radicals are trapped by DMPO in H_2O **(a)** and the photogenerated $•O_2^-$ radicals by DMPO in methanol **(b)**.

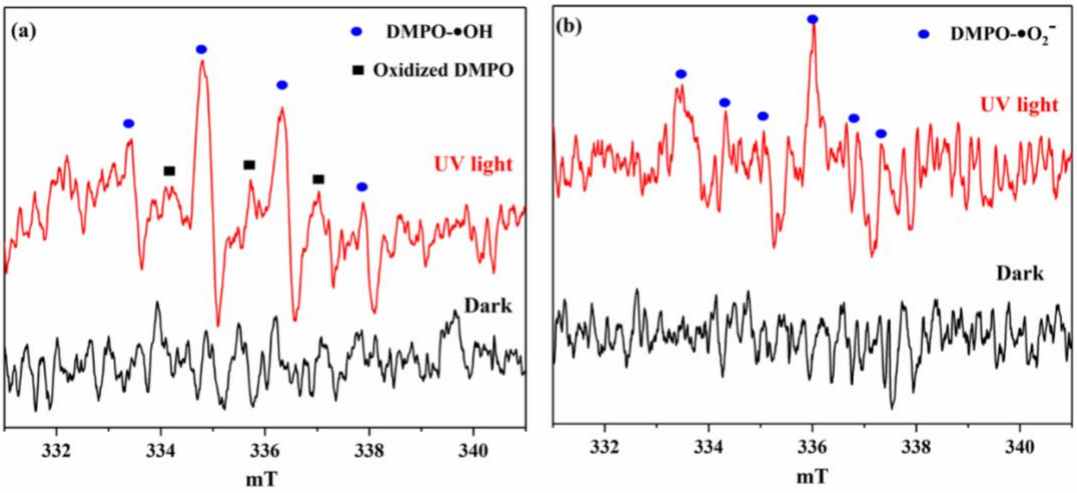

According to literature[S23-S24], the photogenerated electrons and holes on ARM-phase titania catalysts under UV irradiation are expected to react with O_2 and H_2O molecules to form $•O_2^-$ and •OH radicals, respectively, via the following reactions:

$$TiO_2 + hv \rightarrow TiO_2(h^+ + e^-)$$

$$h^+ + H_2O \rightarrow \cdot OH + H^+$$

$$e^- + O_2 \rightarrow \cdot O_2^-$$

Upon UV irradiation, therefore, the titania catalysts to catalyze the sequential oxidative reactions of gaseous acetaldehyde into acetic acid (CH_3COOH) as intermediate products and then into CO_2 and H_2O as final products by using either •OH or $•O_2^-$ or both via the following reactions:

(a) Oxidation pathways of CH_3CHO by using photogenerated $\cdot OH$ radicals:

$$CH_3CHO + \cdot OH \rightarrow CH_3CO\cdot + H_2O$$

$$CH_3CO\cdot + \cdot OH \rightarrow CH_3COOH$$

$$CH_3COOH + 2H_2O + 8h^+ \rightarrow 2CO_2 + 8H^+$$

(b) Oxidation pathwats of CH_3CHO by using photogenerated $\cdot O_2^-$ radicals:

$$CH_3CHO + \cdot O_2^- \rightarrow CH_3CO\cdot + HO_2^-$$

$$CH_3CHO + HO_2^- \rightarrow CH_3CO^- + H_2O_2$$

$$CH_3CO\cdot + H_2O_2 \rightarrow CH_3COOH + \cdot OH$$

$$CH_3CO^- + \cdot OH \rightarrow CH_3COOH + e^-$$
$$CH_3COOH + 2O_2 \rightarrow 2CO_2 + 2H_2O$$

Figure S18 shows the strong characteristic signal of DMPO-·OH species and weak characteristic signals of DMPO-·O_2^- species, which suggests that as compared with the photogenerated •O_2^- radicals, the photogenerated •OH radicals play a dominant role in photocatalysis of as-prepared C-A/R-TiO_2-2.9 powder for oxidative degradation of gaseous acetaldehyde in air with relative humidity of 75%.

C. References

(S1) Z. Jiang, C. Lu, H. Wu, Photo-regeneration of NADH using carbon-containing TiO_2, *Ind. Eng. Chem. Res.*, 2005, **44**, 4165-4170.

(S2) X. Song, Z. Sun, Q. Huang, M. Rettenmayr, X. Liu, M. Seyring, G. Li, G. Rao, F. Yin, Adjustable zero thermal expansion in ati-perovskite manganese nitride. *Adv. Mater*., 2011, **23**, 4690-469.

(S3) D. A. H. Hanaor, C. C. Sorrell, Review of the anatase to rutile phase transformation, *J. Mater. Sci.*, 2011, **46**, 855-874.

(S4) Y. Yang, H. Li, H. Zhao, R. Qu, S. Zhang, W. Hu, X. Yu, X. Zhu, S. Liu, C. Zheng, et. al. Structure and crystal phase transition effect of Sn doping on anatase TiO_2 for dichloromethane decomposition, *J. Hazard. Mater.*, 2019, **371**, 156-164.

(S5) F. Yu, C. Wang, Y. Li, H. Ma, R. Wang, Y. Liu, N. Suzuki, C. Terashima, B. Ohtani, T. Ochiai, A. Fujishima, X. Zhang, Enhanced solar photothermal catalysis over solution plasma activated TiO_2, *Adv. Sci.*, 2020, **7**, 2000204.

(S6) S. Zhang, Y. Zhuo, C.I. Ezugwu, C. Wang, C. Li, S.Liu, Synergetic molecular oxygen activation and catalytic oxidation of formaldehyde over defective MIL-88B(Fe) nanorods at room temperature, *Environ. Sci. Technol.,* 2021, **55**, 8341-8350.

(S7) P. Wang, R. Shi, Y. Zhao, Z. Li, J. Zhao, J. Zhao, G. I. N. Waterhouse, L. Wu, T. Zhang, Selective photocatalytic oxidative coupling of methane via regulating methyl intermediates over metal/ZnO nanoparticles, *Angew. Chem. Int. Ed.* 2023, e202304301.

(S8) P. Wang, J. Zhao, R. Shi, X. Zhang, X. Guo, Q. Dai, T. Zhang, Efficient photocatalytic aerobic oxidation of bisphenol A via gas-liquid-solid triphase interfaces, Mater. Today Energy, 2022, **23**, 100908.

(S9) W. Yuan, B. Zhu, X. Li, T. W. Hansen, Y. Ou, K. Fang, H. Yang, Z. Zhang, J. B. Wagner, Y. Gao, et. al. Visualizing H_2O molecules reacting at TiO_2 active sites with

transmission electron microscopy, *Science*, *2020*, **367**, 428-430.

(S10) T. Sun, E. Liu, J. Fan, X. Hu, F. Wu, W. Hou, Y. Yang, L. Kang, High photocatalytic activity of hydrogen production from water over Fe doped and Ag deposited anatase TiO_2 catalyst synthesized by solvothermal method, *Chem. Eng. J.*, 2013, **228**, 896-906.

(S11) Y. Li, Z. Ren, M. Gu, Y. Duan, W. Zhang, K. Lv, Synergistic effect of interstitial C doping and oxygen vacancies on the photo-reactivity of TiO_2 nanofibers towards CO_2 reduction, *Appl. Catal., B,* 2022, **317**, 121773.

(S12) T. Zhang, J. Low, J. Yu, A. M. Tyryshkin, E. Mikmekov, T. Asefa, A blinking mesoporous TiO2@x composed of nanosized anatase with unusually long-lived trapped charge carriers, Angew. *Chem. Int. Ed.*, 2020, **59**, 15000-15007.

(S13) Q. Zhang, H. He, X. Huang, J. Yan, Y. Tang, H. Wang, TiO2@C nanosheets with highly exposed (001) facets as a high-capacity anode for Na-ion batteries, *Chem. Eng. J.*, 2018, **332**, 57-65.

(S14) Y. Wang, Y.X. Chen, T. Barakat, T. M. Wang, A. Krief, Y. J. Zeng, M. Laboureur, L. Fusaro H. G. , Liao, B. L. Su, Synergistic effects of carbon doping and coating of TiO_2 with exceptional photocurrent enhancement for high performance H_2 production from water splitting, *J. Energy Chem.*, 2021, **56**, 141-151.

(S15) W. Zhou, Y. Liu, Y. Zhang, G. Yang, S. Deng, F. Shen, H. Peng, L. Wang, Novel multi-layer cross-linked TiO_2/C nanosheets and their photocatalytic properties, *New J. Chem.*, 2014, **38**, 1647-1654.

(S16) H. Zhang, Z. Wu, R. Lin, Y. Wang, Exploring the mechanism of room temperature ferromagnetism in C-doped TiO2 nanoclusters by tuning the defects by different annealing temperature using citric acid as C source, *Ceram. Int.*, 2022, **48**, 26836-26845.

(S17) L. Mai, C. Huang, D. Wang, Z. Zhang, Y. Wang, Effect of C doping on the

structural and optical properties of sol–gel TiO_2 thin films, *Appl. Surf. Sci*., 2009, **225**, 9285-9289.

(S18) J. Ding, X. Gao, L. Cha, M. Q. Cai, J. Ma, Synthesis of TiO_2@C nanospheres with excellent electrochemical properties. *RSC Adv*., 2016, **6**, 108310-108314.

(S19) X. Deng, Z. Wei, C. Cui, Q. Liu, C. Wang, J. Ma, Oxygen-deficient anatase TiO_2@C nano-spindles with pseudocapacitive contribution for enhancing lithium storage, *J. Mater. Chem. A*, 2018, **6**, 4013-4022.

(S20) Y. Wen, J. H. Yun, B. Luo, M. Lyu, L. Wang, Tuning the carboncontent on TiO_2 nanosheets for optimized sodium storage, *Electrochim. Ac*ta., 2016, **219**, 163-169.

(S21) H. Liu, W. Li, D. Shen, D. Zhao, G. Wang, Graphitic carbon conformal coating of mesoporous TiO_2 hollow spheres for high-performance lithium-ion battery anodes, *J. Am. Chem. Soc.*, 2015, **137**, 13161-13166.

(S22) J. Torres-Rodríguez, S. N. Myakala, M. Salihovic, M. Musso, N. Hüsing, D. Eder, V. Presser, A. Cherevan, M. S. Elsaesser, Titania hybrid carbon sphero-gels for photocatalytic hydrogen evolution, *Carbon*, 2023, **202**, 487-494.

(S23) I. Sopyan, M.Watanabe, S. Murasawa, K. Hashimoto, A. Fujishima, An efficient TiO_2 thin-film photocatalyst: photocatalytic properties in gas-phase acetaldehyde degradation. *J. Photoch. Photobio. A* 1996, **98**, 79-86.

(S24) Y. Ohko, D. A. Tryk, K. Hashimoto, A. Fujishima, Autoxidation of Acetaldehyde Initiated by TiO_2 Photocatalysis under Weak UV Illumination. *J. Phys. Chem. B* 1998, **102**, 2699-2704.